Modelling and Robust PID-Control of a Shape Memory Alloy Actuated Haptic Finger

Efthymios Kolyvas, Yannis Koveos, George Nikolakopoulos and Anthony Tzes
Electrical and Computer Engineering (ECE) Department,
University of Patras (UoP), Patras 26500, Greece
{*eikolyvas,ykoveos,gnikolak,tzes*}*@ee.upatras.gr*

***Abstract*— The development of (SMA) actuated devices is hindered by the existence of an accurate and yet simplified model. The highly non–linear behavior that is exhibited by these materials does not allow a straightforward application of the classical control strategies met in the field. This current research effort proposes the linearization of a simplified model describing the "shape memory effect" of SMAs and the implementation of a PID controller, which is tuned with the aid of the Linear Quadratic Regulator theory, based on Linear Matrix Inequalities techniques. The proposed scheme is applied to a single–DOF robot manipulator that is activated by two SMA wires and the overall model is controlled via the utilization of the calculated LMI–tuned PID controller. Simulation results are presented that prove the efficacy of the proposed control scheme.**

Index Terms*— *Shape Memory Alloys, Robotic manipulator, Model verification, LMI.

I. Introduction

The implementation of SMAs into a new generation of actuators is an ongoing procedure, aiming on a broader impact on everyday applications. Still, the absence of a "convenient" model, from a controlling point of view, restricts the new applications to simplified control methods. Though, many efforts have been made on capturing the physical phenomena occurring in the transformations presented in SMAs [1–6], the grade of complexity and the micro–mechanical variables used result in an impractical model. The values of the aforementioned constants and variables are not easily tracked, thus the overall model is not easily verified.

The effort on modelling smart materials is an ongoing task and has been approached by different points. Especially the problem of modelling Shape Memory Alloys in a micro–mechanical level has been met in [7–9]. A more advanced approach is encountered in [10, 11], where the implementation of Finite Elements seems to provide the necessary means for capturing most of the physical properties present in Shape Memory Materials.

Smart materials, in general, owe their special properties in the reversible phase transformations easily identified at the microscopic level. The conditions, though within which the transformation may take place depend on both the environmental conditions applied to the material and its inner characteristics. The first group of external stimulation may advert to physical parameters such as existing strain, applied stress, environmental temperature, while the second group of parameters may refer to the lattice orientation, the existence of gaps within the overall structure and so on. As a result, these inherent properties of smart materials are not easily implemented into a single valued function [12]. Thus, a simplified model would utilize the hysteretic stress–strain, or stress–temperature relations resulting in a highly non-linear and hysteretic model.

The aforementioned properties of smart materials apply to SMAs when they exhibit either the "memory" effect or the "superelasticity" effect. The first case applies to the response obtained by the material (SMA) after a thermal stimuli, while operating within the hysteresis loop and the second one applies to the response corresponding to a mechanical (stress induced) stimuli, at operating points above the hysteretic stress–temperature relationship. The lattice energy balance for each of these two cases, as the temperature (energy) operating point moves within and above the hysteresis loop, is different, thus inducing a different macroscopically observed behavior. The potential energy's local minimum is the criterion for the triggering of the martensitic transformation. Each one of the two states possess different values of potential energy under the given environmental conditions. The external supply of energy (heating, application of stress) force the material to undergo a transformation (martensitic or austenitic) in order to reduce the overall energy (free energy) and to acquire a new tranquility point.

The memory effect is characterized by the innate production of stress, so that the material is able to restore its overall original shape. On the contrary, the superelasticity effect is determined by the capability of the material to absorb externally applied forces. The difference in the response of the same material at two different operating points, produces different demands in the modelling of the material.

This current research is concerned with the modelling of the shape memory effect, which allows the employment of SMA as a thermal actuator. In the rest of the paper, the special characteristics of the shape memory transformation and the equations describing the overall behavior of the material are discussed in Section 2. The overall model of the haptic finger is provided in Section 3 while the linearization of the nonlinear dynamical equations is given in Section 3. The tuning of the PID with the aid of the LMIs theory is presented in Section 4, along with the simulation results generated for the closed loop system. Finally concussions are drawn in Section 5.

II. SMA Modelling

The previously described transformation for the smart materials, is also present in the responsible mechanism for the behavior of SMAs. A two way (reversible) transformation is observed between two equilibrium states–the high energy (temperature) state and the lower energy (temperature) one.

The forward transformation is responsible for the transition from the upper temperature state to the lower temperature state and is achieved by the abduction of temperature from the material. Thus, its overall temperature drops from the upper equilibrium state to the lower one $M_s \rightarrow M_f$ (Martensitic starting temperature to Martensitic finishing temperature). The reverse transformation is also possible, from a lower temperature state towards an upper temperature state $A_s \rightarrow A_f$ (Austenitic starting temperature towards Austenitic finishing temperature). The kick–off temperatures for each of the two transformations are different and result in a hysteresis loop similar to the one presented in Figure 1. The stress–temperature curve presented in Figure 1 is typical

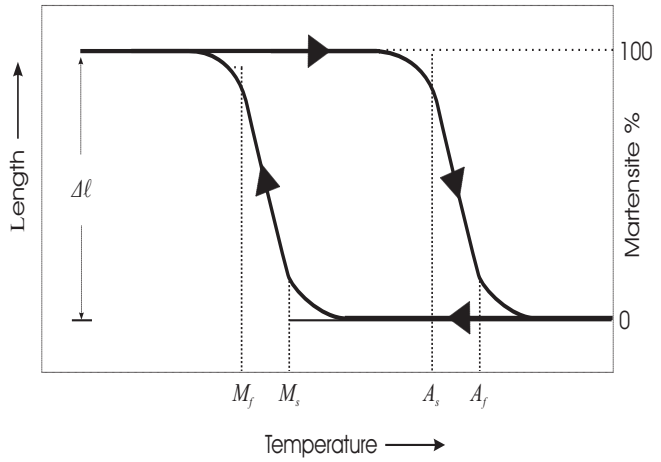

Fig. 1. Typical hysteresis loop met in SMAs

for SMAs exhibiting either the shape memory either the superelasticity phenomenon. These both phenomena exist in SMAs as they are due to the same mechanism, with the only differences that are: a) triggered by different exogenous factors, and b) that they exist under different environmental conditions.

The martensitic transformation is a diffusionless transformation, which when induced in SMAs, results in a reorientation of the parent (previously existing) lattice structure. The mechanism of the lattice reorientation is depicted in Figure 2. The constraint of the non–diffusion and the memory of the atoms' original place upon the lattice is the cause for the reversibility of the phenomenon and the shape memory effect that is macroscopically observed. When the hysteresis loop is shifted above the upper austenitic finish temperature (environmental condition is satisfied), the lattice reorientation occurs in order to relief the material from the additional stress induced. When the additional stress seizes to exist, the material recovers its original lattice configuration and therefore its overall shape.

The inverse phenomenon is applicable in the shape memory effect. The heating induced (different to the previously mentioned environmental variable) upon the material, rises the material's temperature above the corresponding value (A_s) and triggers the ongoing of the transformation. The lattice reorientation results in a different shape, thus producing a value of stress much larger than the one applied for the deformation of the material. The amount of stress obtained,

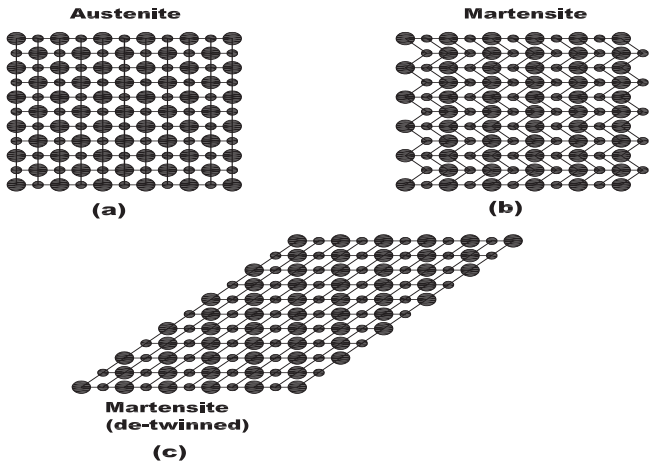

Fig. 2. Lattice reorientation upon transformation

may be described by Hooke's law as stated in [7]:

$$\sigma = E\varepsilon^e = E[\varepsilon - \varepsilon^t - \alpha(T - T_r)] \tag{1}$$

where σ is the unaxial stress produced, ε^e is the elastic strain, ε is the total strain and ε^t is the transformation strain, while E and α are the Young's modulus and the thermal expansion coefficient respectively and may be substituted to the above equation as:

$$E = E^A + \xi(E^M - E^A) \tag{2}$$

and

$$\alpha = \alpha^A + \xi(\alpha^M - \alpha^A). \tag{3}$$

The dominant phase within the material is characterized by the micromechanical variable ξ, which describes the volumetric fraction of martensite upon austenite. Each one of the E and α variables is a function of ξ, as each one of the two states (martensite/austenite) possesses different physical properties. The corresponding values for each state are incorporated in the material and are defined as: a) E^A and E^M for the pure austenitic and pure martensitic materials' Young's modulus, and b) a^A and a^M for the pure austenitic and pure martensitic thermal expansion coefficient respectively.

Since the transformation is explicitly dependent upon the volumetric fraction of martensite and the material is loaded only under tension, the transformation strain is expressed by means of $\xi : \ \varepsilon^t = H\xi$, where H is the maximum axial transformation strain.

The overall transformation phenomenon described by the micromechanical variable ξ is given by the simplified exponential model of Tanaka [13] and two different expressions account for the forward and the backward transformation respectively.

$$\xi_M = 1 - \exp\left[\frac{\ln(0.01)}{M_s - M_f}(M_s - T)\right] \tag{4}$$

for $M_f \leq T \leq M_s$, whereas for the inverse transformation the afforementioned equation becomes:

$$\xi_A = \exp\left[\frac{\ln(0.01)}{A_s - A_f}(A_s - T)\right] \tag{5}$$

for $A_s \leq T \leq A_f$.

Both models presented for the austenitic and the martensitic transformation are experimentally obtained [13] and reveal some weaknesses. The aging effect and the co–existence of multiple martensitic layers, at the same time are not taken into account, therefore a diversion from experimentally obtained results should be expected.

Nevertheless, the dynamic response for an ideal material is accurately captured and the simplicity of the model (there is absence of multiple micromechanics variables, no higher order derivatives are utilized and the switching from the one model–austenitic–to the next one –martensitic– is performed in steady state) allows an easily implementation in a software package and cost effective simulations of the highly non–linear, hysteretic material. The basic drawback of the current model is that the physical constants, such as the H, E_A, E_M, α_A, α_M, etc. must be accurately tuned, when considering the verification with the experimental data.

III. Haptic finger model

In the current research effort, SMAs are utilized as thermal actuators in a haptic finger. More specifically the parameters of the simulation have been tuned in order to match the environmental variables applied in the experimental setup. The operation of the haptic finger may be found in Figure 3, where the placement of the SMA wire, along with the produced forces and torques are presented. The necessary

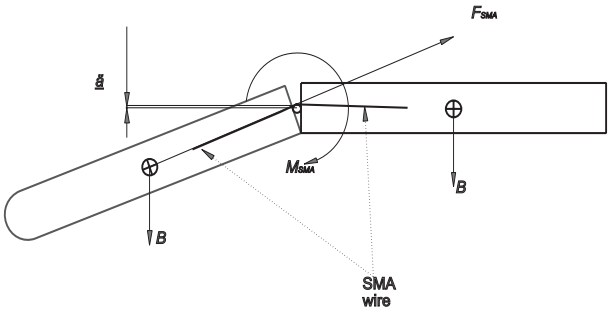

Fig. 3. Free Body Diagram for the single DOF haptic finger

torque is provided by the use of SMA in the role of tendons. The initial configuration of the system forces the tendon to be stressed and deformed due to the link's own weight. By the application of external voltage, the SMA is heated in accordance to Joule's law and the shape memory effect is activated. Each one of the two tendons, that is responsible for the positioning of the link –which are placed at each side of the finger's skeleton, contracts as it undergoes the shape change and produces a magnitude of stress enough to cancellate the effect of gravity on the link. The dynamics of the single DOF haptic finger is:

$$\tau = \frac{Mg\ell\cos(\theta)}{2} + \frac{1}{3}M\ell^2\ddot{\theta}. \quad (6)$$

Equation 7 provides a more accurate description of the process discussed in the previous.

$$F_{SMA}\cdot\delta = \frac{Mg\ell\cos(\theta)}{2} + \frac{1}{3}M\ell^2\ddot{\theta} \quad (7)$$

The constants of the above equations are defined from: a) the distance of the beneficial factor of F_{SMA} from the center of rotation, δ, b) the mass of the link M, d) the horizontal distance of gravity from the rotational center l, and e) the angle written from the link to the horizontal axis θ. The last term of the previous equation is neglected as the dynamics of the system are not involved in the current control issue. Back substitution of the aforementioned equations results in the expected non–linear and hysteretic model.

IV. Dynamics linearization

The main difficulties induced in the current model stem from the nature of the utilized actuator. The stress–temperature response of the SMA may be found in Figure 4.

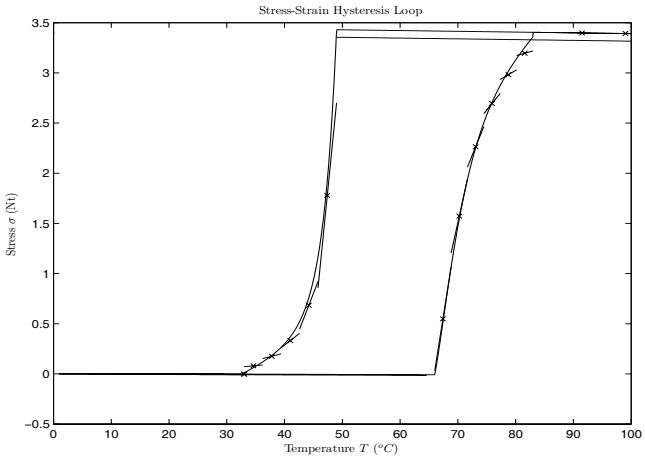

Fig. 4. Stress-Temperature hysteresis with the presence of the linearized systems

The exponential response obtained for the stress–temperature relationship is due to the exponential model of Tanaka [13] which is incorporated into the current model. As previously discussed, the martensitic volume fraction ξ is the micromechanical parameter that is responsible for the triggering of the shape memory effect phenomenon. It takes values between $0 \rightarrow 1$, where 0 represents the pure austenitic state and 1 the pure martensitic state.

The non–linear phenomena are induced by ξ where confronted by linearizing the stress–temperature curve at predefined operating points T^o. The utilized operating points, are presented in Table I.

TABLE I
Operating Points

$T^o_{heating}$	$\sigma_{heating}$	$T^o_{cooling}$	$\sigma_{cooling}$
33	-0.02	99	3.34
67.42	0.55	47.4	1.78
70.25	1.57	44.2	0.84
73	2.26	41	0.33
76	2.7	37.8	0.176
78.75	2.98	34.6	0.08
81.6	3.2	33	-0.002
91.5	3.4	x	x

Table I presents the chosen temperature operating points for the linearization of the heating and the cooling phenomena respectively. Eight linear models were chosen to describe the heating of the material, whereas seven models are capable of describing the cooling process. The stresses predicted by

the model are indicative of the capabilities provided through the use of the specific material. The values of the constants used for the specific simulation are given in Table II.

TABLE II
PHYSICAL PROPERTIES

SMA physical properties			
E^A	69 GPa	E^M	30 GPa
a^A	$11 \times 10^{-6}\ ^oC^{-1}$	a^M	$6.6 \times 10^{-6}\ ^oC^{-1}$
A_s	$66\ ^oC$	A_f	$83\ ^oC$
M_s	$49\ ^oC$	M_f	$33\ ^oC$
H	3.5%	T_{ref}	$23\ ^oC$

Haptic finger properties			
δ	$6.5 \times 10^{-3}\, m$	L	$0.05\, m$
g	$9.81\ \frac{m}{sec^2}$	M	$0.03 kgr$

The block–diagram of the non–linear model in a schematic representation is presented in Figure 5.

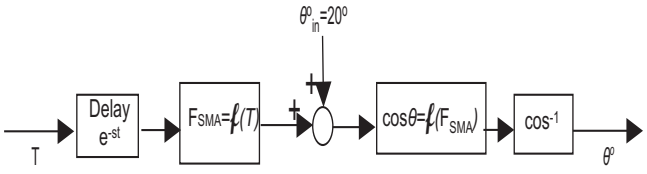

Fig. 5. Topology of the open-loop system

The system's excitation is the temperature and the rotation of the haptic finger is the output of the model. The initial configuration of the robot is chosen as the 20^o below the horizontal axis and the stress induced by the SMA wire results in a final configuration of approximately 5^o below the horizontal axis. The angles that appear in the simulation results that are below the horizontal axis assume a positive sign. The open–loop response of the model is depicted in Figure 6.

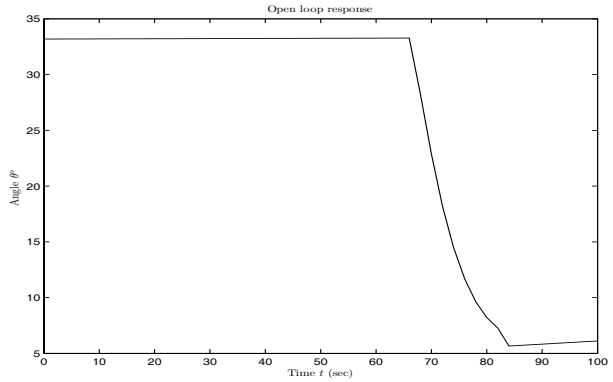

Fig. 6. Angle-Temperature response of the open loop system

The previously described linearization of the stress produced by the SMA with respect to the input–temperature, results in an equation of the form:

$$\delta\sigma = \alpha_{\mathbf{con}} + \beta_{\mathbf{coeff}} \cdot \delta T \tag{8}$$

where the higher powers of δT are neglected. Introduction of the previous equation to the one describing the overall model (7), gives a non–linear expression with respect to θ. The operating point of $\theta^o = 10^o$ is chosen for the linearization of the cosine factor. Thus the linear equation describing the overall model is of the following form:

$$\alpha_\theta \delta\ddot{\theta} - \beta_\theta \delta\theta = \alpha_{\mathbf{con}}\delta \cdot \delta T + \beta_{\mathbf{coeff}} \tag{9}$$

and the set of the constitutive equations yields in:

$$\begin{bmatrix} \delta\dot{\theta} \\ \delta\ddot{\theta} \end{bmatrix} = \begin{bmatrix} 0 & 1 \\ \frac{\beta_\theta}{\alpha_\theta} & 0 \end{bmatrix} \begin{bmatrix} \delta\theta \\ \delta\dot{\theta} \end{bmatrix} + \begin{bmatrix} 0 \\ \frac{\beta_{\mathbf{coeff}}\delta}{\alpha_\theta} \end{bmatrix} \delta T + \begin{bmatrix} 0 \\ \frac{\alpha_{con}}{\alpha_\theta} \end{bmatrix} \tag{10}$$

In the last two equations (9) and (10) $\alpha_{\mathbf{con}}, \beta_{\mathbf{coeff}}$, are the matrices produced for the linearized models around each operating point. Specifically, $\alpha_{\mathbf{con}}$ represents the accumulation of the constant terms present in each model and $\beta_{\mathbf{coeff}}$ the terms of δT.

The closed loop system involves the implementation of a PID controller where the tuning of the K_P, K_I and K_D parameters is accomplished via the utilization of appropriate formulated LMIs [14].

V. LMI BASED PID TUNING

The constitutive model provided by (10) is sufficient for the tuning of the PID controller as discussed in [14]. A state feedback control law of the form:

$$u = -Kx = -R^{-1}B^T P x \tag{11}$$

is assumed for the constitutive model

$$\begin{aligned} \dot{x} &= Ax + Bu \\ y &= Cx \end{aligned} \tag{12}$$

and for the minimization of the LQR quadratic cost:

$$J(u) = \int_0^\infty \left(x^T Q x + u^T R u\right) dt \tag{13}$$

where Q, R are positive semidefinite matrices for the controllable system (sub–systems) (A, B) and P is the solution of the Riccatti equation:

$$A^T P + PA - PBR^{-1}B^T P + Q = 0. \tag{14}$$

The problem of solving the Riccatti equation in (14) is surmounted by the reformulation of (14) with the aid of Shur's complement [15]. Thus the solution of the Riccatti is transformed into its equivalent formulation of finding a matrix P, that satisfies simultaneously the following matrix inequalities:

$$\begin{bmatrix} A\tilde{P} + \tilde{P}A^T + BY + Y^T B & \tilde{P} & Y^T \\ \tilde{P} & -Q^{-1} & 0 \\ Y & 0 & -R^{-1} \end{bmatrix} \leq 0 \tag{15}$$

$$\tilde{P} > 0 \tag{16}$$

$$\begin{bmatrix} \gamma & x^T(0) \\ x(0) & \tilde{P} \end{bmatrix} \geq 0 \tag{17}$$

where $Y = -K\tilde{P}$ and $\tilde{P} = P^{-1}$. The third LMI (17) is incorporated in order to relax the strict constraint of setting the quadratic cost to zero:

$$J_{\min} = x^T(0) P x(0) \tag{18}$$

thus bounding instead the cost J_{min} with a desired value γ.

$$J_{\min} \leq \gamma \tag{19}$$

In our work, γ is a variable of the problem and its minimum value is sought, so as to guarantee the solvability of the set of LMIS (15-17) and the convergence of the algorithm. The proposed control strategy is also valid for a polytopic set of subsystems $\{[A_1, B_1], \ldots, [A_n, B_n]\}$.

The implementation of a static gain state feedback PID controller requires the existence of a triplet of states. Thus the original state space model (10) is augmented with a pseudo-=state representing the error signal. The constitutive model is reformulated to the one shown in (20).

$$\begin{bmatrix} \delta\dot{\theta} \\ \delta\ddot{\theta} \\ -e \end{bmatrix} = \begin{bmatrix} 0 & 1 & 0 \\ \frac{\beta_\theta}{\alpha_\theta} & 0 & 0 \\ 1 & 0 & 0 \end{bmatrix} \cdot \begin{bmatrix} \delta\theta \\ \delta\dot{\theta} \\ -\int edt \end{bmatrix} + \begin{bmatrix} 0 \\ \frac{\beta_{\mathbf{coeff}}\delta}{\alpha_\theta} \\ 0 \end{bmatrix} \cdot \delta T + \begin{bmatrix} 0 \\ \frac{\alpha_{con}}{\alpha_\theta} \\ 0 \end{bmatrix} \tag{20}$$

Incorporation of the constitutive model in (20) to the set of LMIS in (15 -17), produces the static gains of the PID controller as elements of the vector K of (11).

For the aforementioned case, the static gains K_P, K_I, K_D as calculated by the LMI algorithm are given: $K_P = -4.136 \cdot 10^{-4}$, $K_I = 2.573 \cdot 10^{-3}$ and $K_D = 6.64 \cdot 10^{-5}$. The gains of the PID controller provided, assume small values producing thus control signals of small magnitude. The control effort applied for the current system, remains within physically realizable bounds, while excludes the demand for additional constraints on the control signal $u_{\max}$.

The linearization of the model proposed in Section IV, is valid in small regions around the equilibrium point defined in Table I. The control effort produced by the PID controller is also responsible for the fitting of the output around the equilibrium state. Thus a pre–compensator is implemented, in order to transfer the model in a region near a predefined equilibrium. A schematic representation of the closed loop control topology is provided in Figure 7.

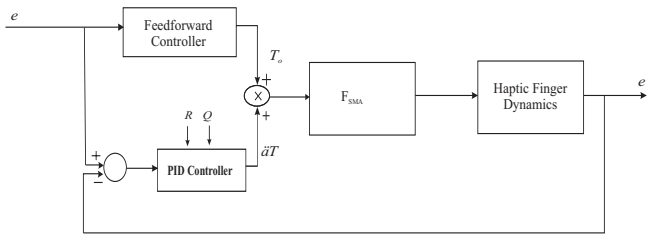

Fig. 7. Topology of the closed loop system

The calibration of the feed–forward controller is performed by the use of the open–loop response of the system and the construction of correlation mapping scheme between the input (temperature T) and the desired output (angle θ). The return mapping scheme is constructed for the expected system response at the operating points T^o chosen in Table I.

VI. Simulation results

The response of the closed loop system for different values of reference inputs is captured in the ensuing Figures.

The time delay observed in the response of the closed–loop system is induced in the modelling of the system in order to account for the delay caused by the heat transfer, which is the main factor for prohibiting the SMAs of a larger bandwidth. The time delay is incorporated in the simulation, as may be found in Figures 8–11 with a value of $0.4sec$, but was not included during the design of the controller. The presence of the delay will be dealt with in a future stage of our work – after the incorporation of the heat transfer problem. The overall model is not influenced by its presence, as the delay is introduced at the input of the model presented previously by Figure 5.

Figures 8–11 depict the angle θ response of the haptic finger, under closed–loop control and a step input as the excitation signal. The value of the excitation is the one corresponding to the desired–reference angle. Thus, the response obtained is the step response of the angle of the finger, starting from the initial configuration of the 32^o and resulting to the desired final configuration of 5^o, 10^o , 15^o and 20^o respectively.

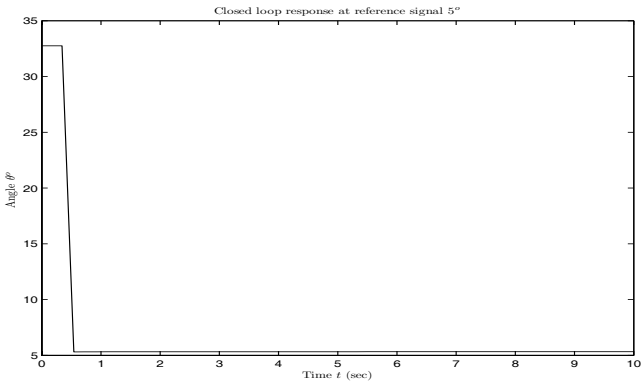

Fig. 8. Closed loop response with 5^o reference signal

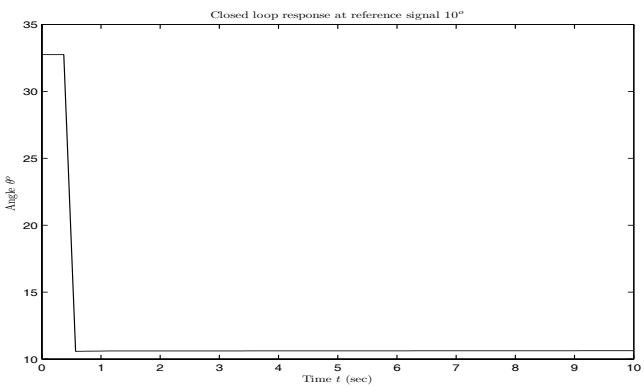

Fig. 9. Closed loop response with 10^o reference signal

In figures 8, 9, 10 and 11 the robustness of the static gain PID controller, tuned with the LMI method is demonstrated. The responses obtained are close to the ones expected, as they are typical for a first-order system.

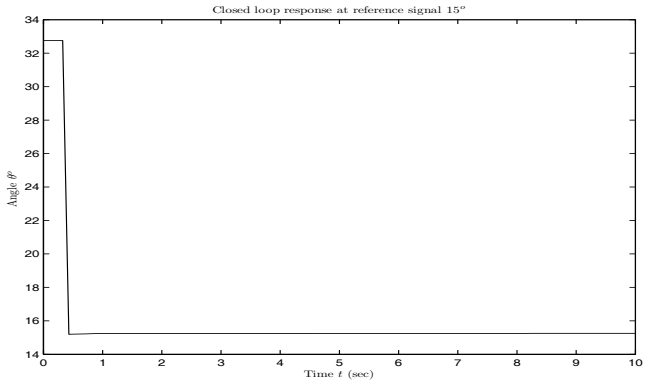

Fig. 10. Closed loop response with 15^o reference signal

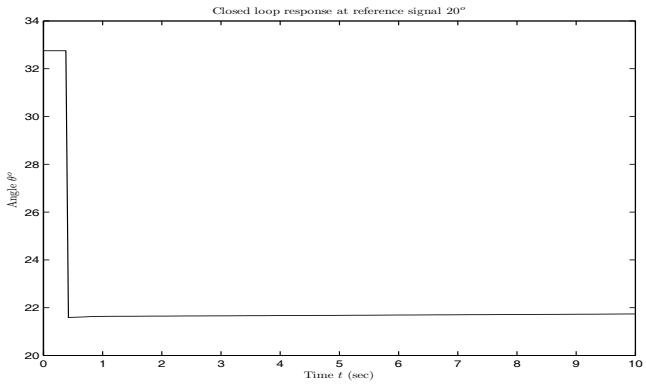

Fig. 11. Closed loop response with 20^o reference signal

The simulation results presented in Fig. 11 reveal the inability of the controller to lead the system to the desired operating point as it is designated by the reference signal (20^o desired angle). This anomaly can be attributed to low accuracy of the linearization procedure as it is depicted in Fig. 4. The linear subsystems responsible for the modelling of the low stress–low temperature operating points of the hysteresis loop of the martensitic transformation and the high stress–high temperature operating points of the austenitic transformation deviate from the response predicted by the non-linear hysteretic model. Thus, the linear sub-systems fail to provide the nominal stress predicted by the "real system" and the resulting torque is insufficient for elevating the haptic finger to the desired final value. Despite the latter observation, the response obtained by the closed–loop system provides the necessary means for moving on the coupling procedure with the experimental setup.

VII. Conclusions

The special characteristics revealed by the use of SMAs cannot be fully exploited, unless a standardized control strategy can be applied. The process of linearizing the simplified model chosen, proves to be an accurate solution to the effort of implementing a PID controller that it is tuned in the LMI sense.

A more extensive model will include the heat transfer and conducting process of SMAs and the proper tuning of the constants met in the current model in order to achieve an agreement with experimental data. A simplified, yet accurate, model is pursued so that more sophisticated control techniques can be applied.

References

[1] Z. B. M. Brocca, L.C. Brinson, "Three dimensional constitutive model for shape memory alloys based on microplane model," *Journal of the Mechanics and Physics of Solids*, 2000. (submitted).

[2] S. H. X.Peng, Y. Yang, "A comprehensive description for shape memory alloys with a two-phase constitutive model," *International Journal of Solids and Structures*, 2001.

[3] G. H. S. Govindjee, A. Mielke, "The free energy of mixing for n-variant martensitic phase transformations using quasi-convex analysis," *Journal of the Mechanics and Physics of Solids*, 2002.

[4] R. R. Y. Jung, P. Papadopoulos, "Constitutive modelling and numerical simulation of multivariant phase transformation in superelastic shape-memory alloys," *International Journal for Numerical Methods in Engineering*, 2004.

[5] J.G.Boyd and D.C.Lagoudas, "A thermodynamic constitutive model for the shape memory materials. part i. the monolithic shape memory alloys," *International Journal of Plasticity*, 1994.

[6] J.G.Boyd and D.C.Lagoudas, "A thermodynamic constitutive model for the shape memory materials. part ii. the sma composite materials," *International Journal of Plasticity*, 1994.

[7] S.G.Shu, D.C.Lagoudas, D.Hughes, and J.T.Wen, "Modelling of a flexible beam actuated by shape memory alloy wires," *Journal of Smart Materials and Structures*, pp. 265–277, 1997.

[8] R. C. Fr.E. Fujta, *Physics of New Materials*. Berling-Springer, 1998.

[9] S. M. M. Fremond, *Shape Memory Alloys*. Springer-Verlag Wien New York, 1996.

[10] P. P. C.A.P.L. La Cava, M.A. Savi, "A nonlinear finite element method applied to shape memory bars," *Journal of Smart Materials and Structures*, 2004.

[11] J. Mackerle, "Smart materials and structures: Fem and bem simulations a bibliograhy (1997-1999)," *Finite Elements in Analysis and Design*, 2001.

[12] R.V.N.Melnik, A.J.Roberts, and K.A.Thomas, "Phase transitions in shape memory alloys with hyperbolic heat conduction and differential–algebraic models," *Computational Mechanics*, vol. 29, pp. 16–26, 2002.

[13] A.Bhattacharyya, D.C.Lagoudas, Y.Wang, and V.K.Kinra, "On the role of thermoelectric heat transfer in the design of sma actuators:theoretical modelling and experiment," *Journal of Intelligent Materials and Structures*, 1995.

[14] Q. W. M. Ge, M. Chiu, "Robust pid controller design via lmi approach," *Journal of Process and Control*, vol. 12, pp. 3–13, 2002.

[15] R. B. J. VanAntwep, "A tutorial on linear and bilinear matrix inequalities," *Journal of Process Control*, vol. 10, pp. 363–385, 2000.